Analysis the MICADO-MAORY SCAO performance

Fabrice Vidal[a], Milan Rozel[a], Vincent Deo[a], Florian Ferreira[a], Arnaud Sevin[a], Eric Gendron[a], Yann Clénet[a], Damien Gratadour[a], Gérard Rousset[a] and Richard Davies[b]

[a] LESIA, Observatoire de Paris, Université PSL, CNRS, Sorbonne Université, Université de Paris, 5 place Jules Janssen, 92195 Meudon, France
[b] Max-Planck-Institut fur Extraterrestrische Physik, Garching, Germany

ABSTRACT

MICADO is the ELT near-infrared first light imager. It will provide diffraction limited images thanks to multi-conjugate adaptive optics (MCAO) and single-conjugate adaptive optics (SCAO) modes provided inside the MAORY module. The SCAO capability is jointly developed by MICADO and MAORY consortia and is motivated by scientific programs for which SCAO will deliver the best AO performance (e.g. exoplanets, solar system science, AGNs, etc) even for very faint objects. Numerical simulations were therefore required to assess the overall performance and explore WFS design parameters and associated calibration procedures. This study concluded to choose a Pyramid WFS (PWFS) working in the visible as the baseline for SCAO mode.

We discuss the specific developments (PWFS diffractive model, ELT pupil shape, M4 geometry and influence functions, telescope perturbations...) implemented in the COMPASS simulation tool to achieve a fast and accurate ELT scale simulation. Thanks to its speed of computation we were able to span quickly a very large parameters space at the ELT scale. We explore the optimizations performed to deal with PWFS specific calibrations expected at the telescope (modal Basis, optical gains, NCPA management, island effect). We present a detailed error budget for each of the 5 turbulence conditions (seeing from 0.47" to 1.13") and guide star magnitudes between 10 to 17 (unresolved single star). We also studied the case of extended objects such as double stars or disk like source objects such as Titan. We finally conclude on the impact on performance using such extended objects for SCAO and PWFS.

Keywords: adaptive optics, wavefront sensing, ELT

1. INTRODUCTION

MICADO is the first light near-IR camera (0.9-2.5μm) on the E-ELT. It has been designed to work at the diffraction limit over a 1' field of view[1] and will come with a long slit spectroscopic mode, at a moderate spectral resolution (5000 to 10000). The Adaptive Optics (AO) correction is supplied by the Multi Conjugate Adaptive Optics (MCAO) module called MAORY.[2] For full scientific exploitation and in a phased approach for developing AO performance at the E-ELT, a SCAO mode is needed for MICADO. It is a joint development between the MICADO and MAORY consortia, integrated into MAORY. This SCAO module will use the built-in deformable mirror (DM) of the E-ELT, the so-called M4 mirror, and a dichroic will send the visible light to the SCAO WaveFront Sensor (WFS). The MCAO module will deliver a moderately high Strehl ratio over the entire 75" field of view while the SCAO mode will provide better on-axis Strehl ratio. We focus in this paper on the latest numerical simulations dedicated to the SCAO mode.

2. SIMULATION PARAMETERS

We present in this section the main AO simulation parameters (turbulence, telescope, deformable mirror and WFS) used with the AO simulation tool COMPASS[3] for all the results presented throughout the paper.

2.1 Turbulence parameters

The simulated turbulence conditions were derived from the ESO specifications and computed at 30° of zenith and summarized in Table 1. Five atmospheric conditions were simulated, each with a different seeing, wind speed and $C_n^2(h)$ profile spread in 35 different layers. The outer scale (L_0) was set to 25m for all layers and turbulence conditions.

Conditions	Seeing (")	r0 (cm)	v_0(m/s)	τ_0 (ms)	# Layers
Q1	0.471	21.47	9.1	8.08	35
Q2	0.619	16.33	9.13	6.12	35
Median	0.702	14.4	9.21	5.35	35
Q3	0.793	12.75	9.13	4.78	35
Q4	1.136	8.9	9.79	3.71	35

Table 1. Summary of simulated turbulence conditions

2.2 Telescope parameters

The E-ELT has a very specific pupil shape. Depending on the field of view angle, the shape and size of the output pupil varies. For the SCAO, working on-axis (or close to) the simulated pupil is dodecagonal and has a diameter of 38.542m with a central obscuration of 0.28 and the width of the E-ELT spiders is 51cm. This particularity leads to a discontinuity of phase partially measured by the wavefront sensor (see Section 4). Figure 1 shows the simulated pupil with the WFS sub-apertures and actuators location.

2.3 Deformable mirror parameters

The M4 unit[4] of the ELT provides a real-time wavefront correction capability. The SCAO mode of MICADO uses this deformable mirror for its own AO correction. M4 is made of 6 different petals and has a total of 5352 actuators. However, since SCAO is only used on-axis, a large number of actuators are hidden by the outer edge pupil + central obscuration. In our case the (useful) total number of actuators simulated is 4300. The M4 actuators geometry is non-squared but rather a non-usual hexagonal pattern. The pitch of the DM is 0.535 cm expressed in the ELT pupil plane. As a side effect, this hexagonal pattern allows a slightly better density of actuators in the pupil plane compared to a squared geometry, increasing the size of the AO correction. Therefore the E-ELT PSFs features a specific hexagonal correction zone in the image plane.
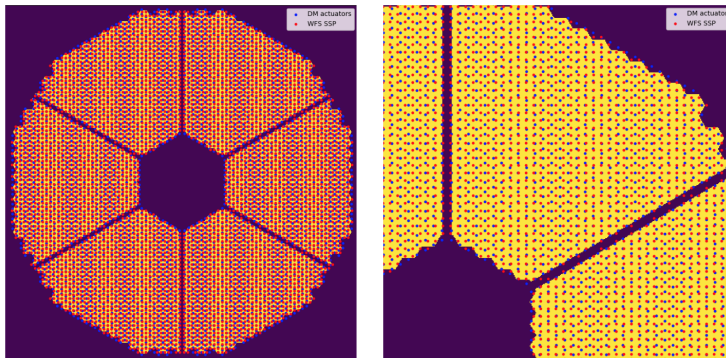

Figure 1. Geometry of the simulated ELT pupil. Center of PWFS sub-apertures are represented in red as well as the center of the DM actuators in blue.

For implementation reasons we did not use the influence functions provided by ESO data. Instead we used Schwartz-like influence functions having the property to combine a fast but smooth descent to zero, with all n^{th} derivatives defined and doing so as well. This allowed us to create influence functions in much smaller support

than the total pupil size (for memory usage) and avoid artificial artifacts in the PSF image due to discontinuities in the DM phase support. Finally, the Tip-Tilt is made on a separated mirror that produces a pure TipTilt and emulates the M5 Mirror. However the emulation of the low band pass (10 Hz) of M5 hasn't been implemented, i.e the Tip tilt separation in frequency between M4 and M5 wasn't simulated. The DM fitting error $\sigma_{fitting}$ (in radians) can be computed using the expression:

$$\sigma_{fitting}^2 = \alpha \frac{pitch}{r_0}^{5/3} \tag{1}$$

With a squared DM geometry, we usually use α=0.232 while with the ELT hexagonal pattern we found our simulations matching the fitting error with α=0.2. With a M4 pitch of 0.53cm, this leads to a fitting error of 106 nm rms under median turbulence conditions (r_0=0.144m at 500 nm).

2.4 WFS parameters

The MICADO SCAO WFS wavelength bandwidth ranges from $0.589\mu m$ (cut below by the MAORY LGS dichroic) to $0.960\mu m$ (left for MICADO science) but the simulated wavelength was monochromatic centered at $0.7\mu m$. Based on previous simulation campaign's we found that a Pyramid wavefront sensor (PWFS[6]) with a $5\lambda/D$ modulation is optimal for most of the encountered conditions (seeing and SNR). The simulated detector is based on the ESO-ALICE camera specification. This detector has a size of 240×240 pixels allowing to form 4 images of the pupil of 92×92 each with only 0.1e- Read Out Noise (RON) at the MICADO AO loop speed specification (500Hz). Note that we choose to use instead a RON=0.3e- based from our measurements on a similar detector (OCAM measurements on the CANARY experiment).

2.5 AO parameters

The SCAO loop is running at baseline a frequency of 500Hz with a 2 frames delay (4ms). The total throughput is 14% which includes atmosphere transmission, telescope, MAORY relay, SCAO Dichroic, SCAO WFS transmission, Quantum Efficiency (QE) at 700nm and a factor of 0.5 for the excess noise of the detector. The zero point is set to 2.6e10 photons/s/m^2. For the temporal filtering we only used an integrator based modal controller with gains.

3. AO CALIBRATION PROCEDURE

We present in this section the calibration procedure we typically follow to optimize the AO loop residuals when using a Pyramid WFS.

3.1 Modal reconstruction

The first calibration step is to define a set of modes used to control actuators space composed of 1 deformable (i.e. the emulated M4) and a pure Tip-Tilt Mirror (emulated M5). We decide to filter the TT and piston from the DM space. This is performed by computing the geometric covariance matrix Δ based on all the Influence Functions of the DM actuators (IF) defined for all the phase points N_ϕ such as:

$$\Delta = \frac{1}{N_\phi}(IF^t.IF) \tag{2}$$

The dimension of Δ is therefore $N_{actus} \times N_{actus}$.

Then we build a matrix T_p ($N_\phi \times 3$) containing the phase corresponding to a pure piston an Tip Tilt and project it onto the IF basis to compute the coefficients τ of those modes onto the IF basis:

$$\tau = \Delta^{-1}.IF^t.T_p \tag{3}$$

Now, we have to generate a set of generators G from IF that cannot produce those modes:

$$G = Id - \tau \left(\tau^t . \Delta . \tau\right)^{-1} . \tau^t . \Delta \tag{4}$$

where Id is the Identity matrix.

The diagonalization of $G^t . \Delta . G$ provides a basis B' and its corresponding eigenvalues λ.

After truncation of the last 3 columns of B' (piston + TT) we have the DM actuator modal basis B:

$$B = G.B'.L \tag{5}$$

with L a matrix with $1/\sqrt{\lambda}$ on its diagonal and 0 elsewhere.

At this point we built a modal basis matrix that cannot produce TT and piston on the DM actuator space. However the final modal basis B_{TT} includes a TT capability on its dedicated mirror is built such as:

$$B_{tt} = \begin{pmatrix} & & & 0 & 0 \\ & \mathrm{B} & & \vdots & \vdots \\ & & & 0 & 0 \\ 0 & ... & 0 & \frac{1}{\mu} & 0 \\ 0 & ... & 0 & 0 & \frac{1}{\mu} \end{pmatrix} \tag{6}$$

where μ are the Tip and Tilt eigenvalues of the geometric covariance matrix of the TT modes Δ_{TT} (2×2 matrix):

$$\Delta_{TT} = \frac{1}{N_\phi}(TT^t . TT) \tag{7}$$

Such a modal basis as therefore the following summarized properties:

- The modes span the full DM space.

- The modes are ordered by increasing spatial frequency.

- The modes are normalized.

- They are orthogonal (their scalar product over the pupil area is null).

- The DM modes are orthogonal to piston and TipTilt.

- The TT modes are purely produced with a dedicated mirror.

3.2 Pyramid WFS optical gain compensation

The optical gain in currently a "hot topic" for SCAO systems using a PWFS on ELTs. The regime under the PWFS will work for MICADO is very different from the ones previously used on various 8-10m class telescopes. Extreme AO systems with PWFS such as SCExAO at Subaru[9] or FLAO at LBT[10] can take advantage of a high spatial resolution sampling (DMs pitch=25cm for FLAO, 18cm for SCExAO) that improves the fitting error and thus maximize the SR allowing the PWFS to work under median turbulence regime with a diffraction limited in the visible core at the pin of the Pyramid. The ELT first generations instruments will use the M4 mirror with a fixed pitch of 54cm which gives a fitting error ranging from 76nm (Q1 turbulence condition) to 158rms (Q4) and above. This leads to SR typically lower than 20% at the PWFS wavelength (R band). Even when the loop is closed it yields to the regime where the PSF starts to enlarge and therefore reduces the performance of the PWFS wavefront reconstruction compared to a diffraction limited core sensing[7] . The optical gain is naturally applied on the controlled modes and reduce their sensitivity which, in the end, result in an under optimized performance.[11] The goal of this optical gain modal compensation (named generically OGMC) is therefore to find the dependency of these modal gains with respect to the (unknown) actual shape "seen" by the PWFS.

Several methods can be used to compute the optical gain, such as proposed by Korkiakoski,[8] dithering on well chosen modes,[12,13] using a deconvolution model based from images of a camera located after the Pyramid modulation[14] or only using the slopes telemetry[15] .

Regardless of the method, the optical gain features a very typical signature depending on the spatial frequencies of modes. Figure 2 shows the AO loop performance for both flat (unoptimized) modal gains or optical gains compensated gains (OGMC) with a seeing of 1.13" (Q4) and integrator gains between 0.2 and 1.6. We also spanned the guide star magnitudes from 9 to 17. It is clear that when using flat gains (dashed lines), the integrator value providing the best performance is reached at gain >1. This can be explained because the integrator gain usually used to optimize the temporal behavior of the loop is here also compensating for the average optical gain of the AO loop. Conversely, when compensating for the optical gain the best performance for each magnitude is this time reached around 0.4 integrator gain. The modal optical compensation successfully compensates the spatial part and leaves the temporal aspect to the integrator. The overall improvement of performance is presented in Figure 3 from magnitudes 9 to 17 with (plain line) or without OGMC (dashed line). At mag 15, the improvement is 12% SR points (SR=28% vs. 41%, in K Band) or 210nm rms. We also dedicate in this paper a section (Sec. 7) to the impact of optical gain compensation on extended objects.
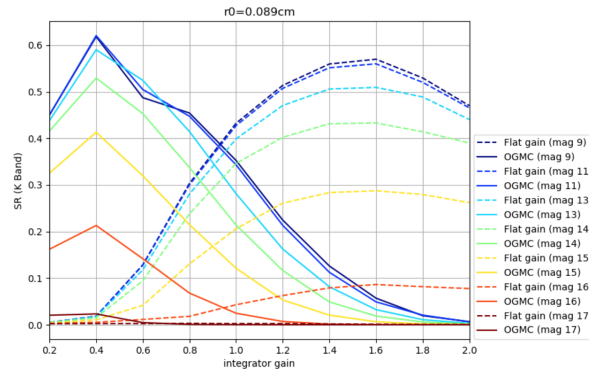

Figure 2. AO loop performance with (plain) and without (dashed) optical gain compensation Vs integrator gain for a Q4 seeing conditions (1.13")
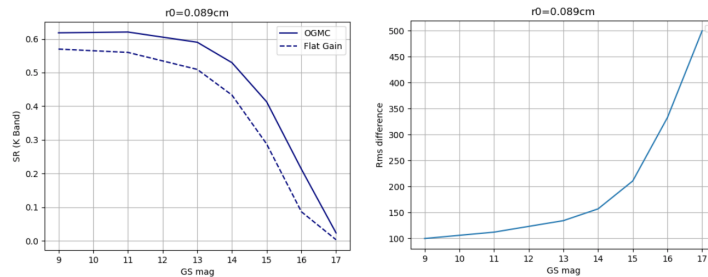

Figure 3. Left: AO loop performance (SR in K Band) vs. Guide star magnitude after with optical gain compensation(OGMC - plain line) and without optical gain compensation (dashed). Right: Rms difference of OGMC vs. Flat Gain for each magnitude (seeing=1.13" - r0=0.089cm).

4. ISLAND EFFECT

The ELT pupil has large spiders that divide its surface into 6 distinct areas, also corresponding to the petals of M4, that are nearly independent from the point of view of the wavefront reconstruction because the width of the spiders is larger than the sub-aperture size and the coherence length of the turbulence. This leads to

an indetermination of the piston mode on each of the petals of M4 also known as *island effect*[5] or *petalling* depending on authors.

Several strategies can be imagined to filter out the differential pistons[16] . One of them, a brutal approach, consists to force the phase continuity by "slaving" the actuators pair-wise on each side of the spiders. Such a solution is presented in Figure 4 where we pair the actuators (in orange) while leaving the others untouched (in blue). With the ELT geometry this leads to a number of 156 actuators slaved, thus having 26 couples of actuators per spider. This slightly reduces the number of modes from 4197 to 4041 which, for a seeing 0.79", marginally increase the fitting error from 118nm rms to 120nm rms. The results with the slaved actuators method is presented in Figure 5 and compared to the case without spiders. The actuator slaving does indeed help to reduce significantly the petalling effect. We find the best performance with slaving actuators gives a SR=71% (total error of 205nm rms) compared to SR=81.9% without spiders (total error = 156nm rms), the Island effect error term is therefore 133nm rms. Despite being a not perfect solution, the evolution of the pistons is now much closer than the expected values of the reference case.
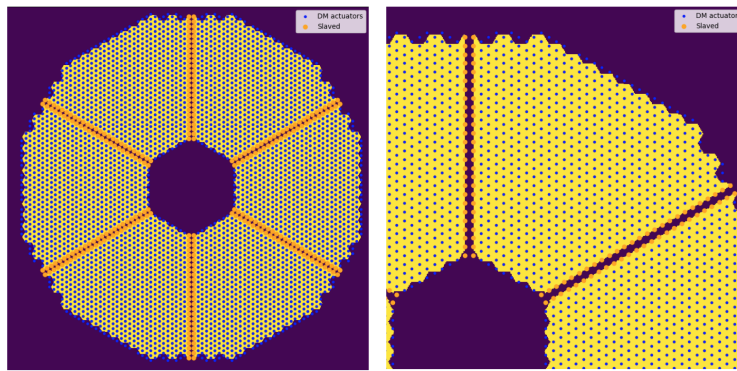

Figure 4. Illustration of the slaved actuators (orange) pair-wise on each side of the spiders. A total of 156 actuators are coupled along the spiders.
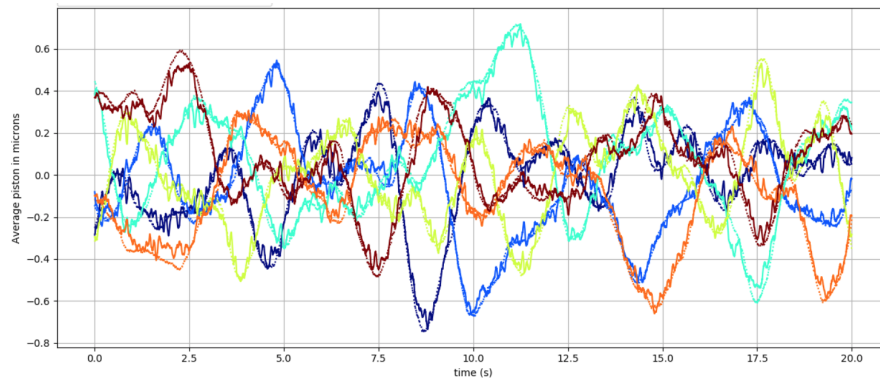

Figure 5. Pistons amplitude measured for each of the 6 petals of the ELT pupil (plain lines: with spiders and slaving actuators method, dotted lines: No spiders)

5. NCPA COMPENSATION

Non Common Path Aberrations (NCPA) compensation is a classical procedure encountered in any adaptive optics systems. The usual way to correct for it is to introduce an offset in the WFS signals (slopes measurements) corresponding to the opposite of the desired aberration to correct. This method has very good results when the

WFS measurements are linear within the range of the NCPA amplitude. However for a Pyramid WFS this linear range is very limited.

For MICADO, the overall NCPA total to correct for is 212 nm rms (loss of 31% SR at 2.2μm) which is, alone, larger than the total allocated budget if nothing is done. The baseline strategy for NCPA compensation is to cancel out most of the low order static parts using a manufactured phase plate located in the SCAO WFS path and manage part of the remaining part using reference slopes on the PWFS. We estimate that after the (partial) cancellation by the phase plate, the PWFS has to handle 86nm rms of aberrations. To make sure this strategy is valid we studied the impact of the NCPA compensation with a PWFS and characterize at which point PWFS stops handling it.

To do so, we simulated Zernike modes from astigmatism (mode #5) to Zernike #30. These are expected to be residuals errors from phase diversity error measurements, phase plate manufacturing error and variable low order aberrations that cannot be compensated with a phase plate only. We spanned their amplitude by changing their total amplitude from 0nm rms to 200nm rms to compute the NCPA wavefront to be corrected on the target. In order to measure the reference slopes from the NCPA wavefront map we use a simulation feature allowing us to show the NCPA phase directly on the WFS. This allows us to directly measure the reference slopes on this non-null zero position without having to perform a phase diversity algorithm from the camera image. Once the reference slopes are measured on the PWFS we remove the NCPA phase on the WFS path and apply it on the imaging (target) path.

As we already introduced in section 3.2, the optical gain plays here a crucial role in the AO performance optimization with PWFS. The same logic actually applies when trying to compensate for static aberrations (i.e. NCPA aberrations). The ability of the PWFS to compensate for a given static mode is also affected by the non-linearity measurements of the PWFS caused by the shape of the PSF (thus the AO loop performance). Applying the reference slopes "as is" during the AO loop degrades the performance in a much more dramatic manner than doing nothing. In other words, it is a much-preferred solution not to try to compensate for NCPA via reference slopes when the NCPA optical gain is not known or cannot be measured in a proper way. In fact, applying the reference slopes without optical gain over-applies its own correction which leads to an instability of the loop decreasing dramatically the final AO performance. To overcome this problem, we estimate the optical gain by measuring the NCPA mode sensitivity during the loop closed. The NCPA mode is only an additional mode we need to measure and compensate for its loss of sensitivity during the loop closed.

By applying the measured NCPA optical gain (here measured using Korkiakoski 's method) on the reference slopes we can now improve the performance without losing in loop stability. Figure 6 presents the AO performance (SR measured in K Band) versus the NCPA amplitude under median seeing conditions. We plot the uncompensated case (in blue) and the reference slopes + optical gain compensation case (in orange). For the MICADO SCAO case (baseline = 86 nm rms NCPA amplitude residuals left on the PWFS), we measure with the reference slopes method a SR= K Band of 85.6% while the uncompensated case gives 81.1%. The 86 nm rms NCPA aberrations are reduced to down 38 nm rms. Under large NCPA amplitude of 200nm rms the reference slopes compensation method still gives SR=82% while no compensation gives SR=67.1% which gives us some margin in case the uncorrected residuals left by the phase plate are larger than expected.

6. SCAO ERROR BUDGET

We present in this section the error budget of the SCAO system using a point source like as guide star. In particular we simulated a "full case" in which, in addition to the turbulence, also compensate for NCPA amplitude of 85nm rms (see also section 5), 123nm rms of windshake perturbation (computed from AO residuals seen after the cascade AO scheme during ELT handover) and manage the Island effect via the slaving technique (see section 4). We performed these simulations for each of the 5 atmospheric conditions (see section 2.1) and also explored the SCAO performance as a function of the guide star magnitude from 9 to 17 (Figure 7). Table 2 details the overall error budget at magnitude 10 for each of the turbulence condition. Under median condition seeing SCAO delivers 69% SR in K band which gives a total residual of 213nm rms (specification is 60%). This term includes fitting, aliasing propagation and bandwidth error + NCPA residual errors + windshake residuals + Island effect error term.
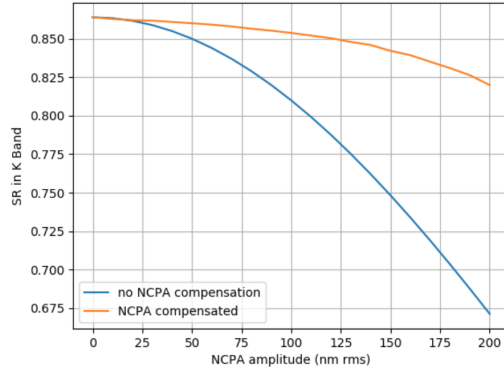
Figure 6. Left: Total wavefront error vs. NCPA amplitude (blue: without NCPA compensation, orange with NCPA reference slopes and optical gain compensation).
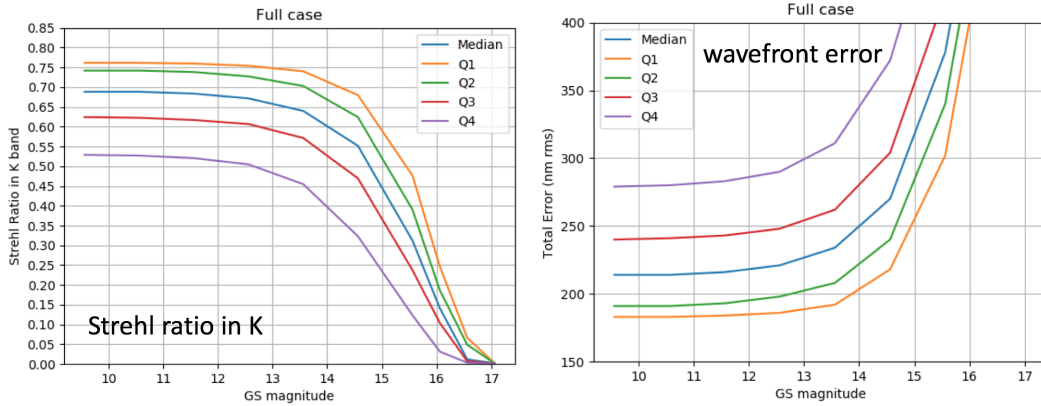

Figure 7. MICADO SCAO performance (left: SR in K band, right: wavefront error in nmr rms) Vs guide star magnitude for each turbulence conditions.

ErrorTerm	Q1	Q2	Median	Q3	Q4
BW + Noise + Aliasing	71	75	88	105	183
Fitting	83	96	106	118	158
Petalling	83	103	125	133	186
Windshake	97	97	97	97	97
NCPA	38	38	38	38	38
Total Error (nm rms)	173	190	213	231	322
SR (K Band)	76.1	74.1	68.8	62.4	58.8

Table 2. SCAO error budget at magnitude 10 for each of the turbulence conditions (Q1 to Q4).

7. EXTENDED OBJECTS AND PYRAMID WFS

This section study the impact on guiding using extended objects with a Pyramid WFS. It is highly driven by the MICADO specifications for which the AO loop shall remain closed for objects <1". It is important to note that all the results presented in the following section does NOT include NCPA, windshake nor Island effect correction. In other words those effects were NOT implemented on extended objects simulation campaigns.

7.1 Practical software implementation

We simulated extended objects by taking advantage of the parallelization of modulation points at the focal plane of the PWFS. Figure 8 *left* represents the single star case implementation with a modulated beam of $5\lambda/D$ using 32 modulation points each separated by λ/D. Figure 8 *center* shows a double star implementation (same $5\lambda/D$ modulation) with an arbitrary separation (center to center) and azimuth, i.e the angle of the double star baseline with respect to the pyramid edges (horizontal and vertical blue lines). It is also possible to simulate a non equal difference of magnitude between the 2 components by simply multiplying the relative weight of each points. Finally, Fig. 8 *right* represents the fully paved disk implemented to simulate an equivalent large and uniform extended object such as Titan ($200\lambda/D$ of diameter). The latter uses 33317 modulation points (!).
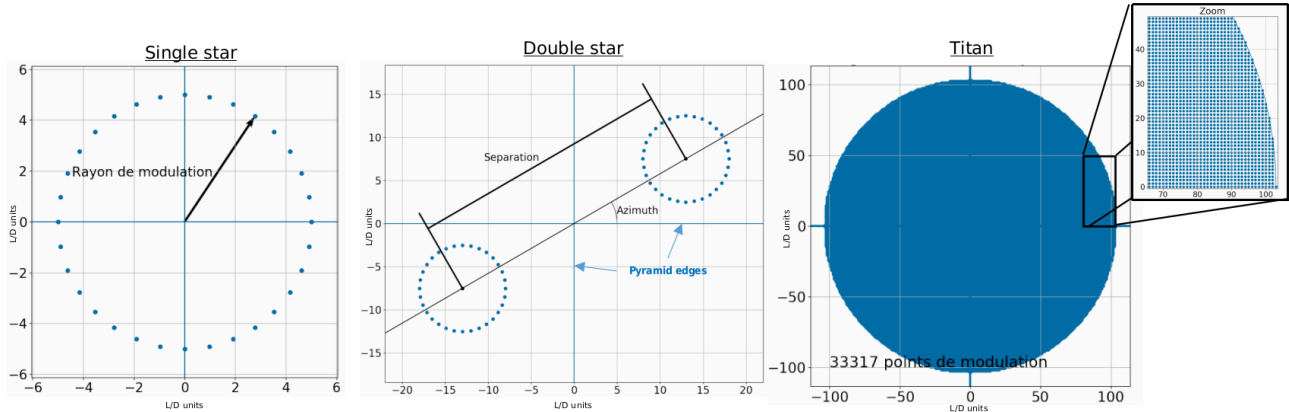

Figure 8. Software implementation of extended objects and Pyramid WFS. We represent the simulated PSF location at the PWFS focal plane. Left: the single star case with a $5\lambda/D$ modulation. Middle: Double star case with an arbitrary component separation and azimuth angle with respect to the Pyramid edges ($5\lambda/D$ modulation). Right: Titan case with 33317 modulation points paved in an homogeneous disk surface.

7.2 Sensing on double stars

We simulate a SCAO PWFS system sensing on a double star with a 8m telescope. We explore the AO performance in a range of separation between 0 and $30\lambda/D$ which, for a 8m telescope gives a maximum separation of 0.54". The result of the simulation is presented in Figure 9 left in which we present the SR in K Band Vs the separation of the double star (in λ/D units or arcseconds separation). The azimuth angle is set to 0 degree (double star separation aligned along the horizontal edge of the pyramid) and the 2 stars have an equal illumination. We studied 2 cases: one *without* optical gain compensation (called FLAT gains - grey line in Fig. 9) and one *with* optical gain compensation using the CLOSE[15] method (blue line in Fig. 9 left). We first see that the 2 curves (with and without OGMC) follows a pretty similar shape and are pretty flat. In particular the AO performance is constant (SR=85%) in the range 0-10λ/D. Beyond 10λ/D of separation the performance slowly decreases. At a separation of 0.54" the Strehl ratio is 78% (K Band) without optical gain compensation, while using OGMC (CLOSE gains) we improve the performance by only 2% (SR=80%). This clearly demonstrates that the need for optical compensation on a 8m telescope is not required since the PWFS works already in a good linear regime.

We now perform the same set of simulations at the ELT scale with the same separation parameters. The result is presented in Figure 9 right. Again we studied the cases *with* (grey) and *without* optical gain compensation (2 OGMC methods compared: CLOSE gains in blue and interpolated gains orange in Fig. 9 right). One clearly see that on a 39m telescope the performance at 0.54" is now affected by optical gains and dramatically drops from 85% to 56.5%. Using optical gains compensation however (either CLOSE or interpolated) helps to reduce the loss of performance at SR=77%, I.e similar to the 8m case. This demonstrates that the need for an optical compensation on a ELT class telescope *is* now fully required. We also clearly distinguish 3 distinct performance regimes as illustrated in Figure 10. The first plateau between 0 and $10\lambda/D$ occurs when the 2 stars are still crossing the Pyramid edges (which is where the wavefront sensing occurs). The second plateau is between 10
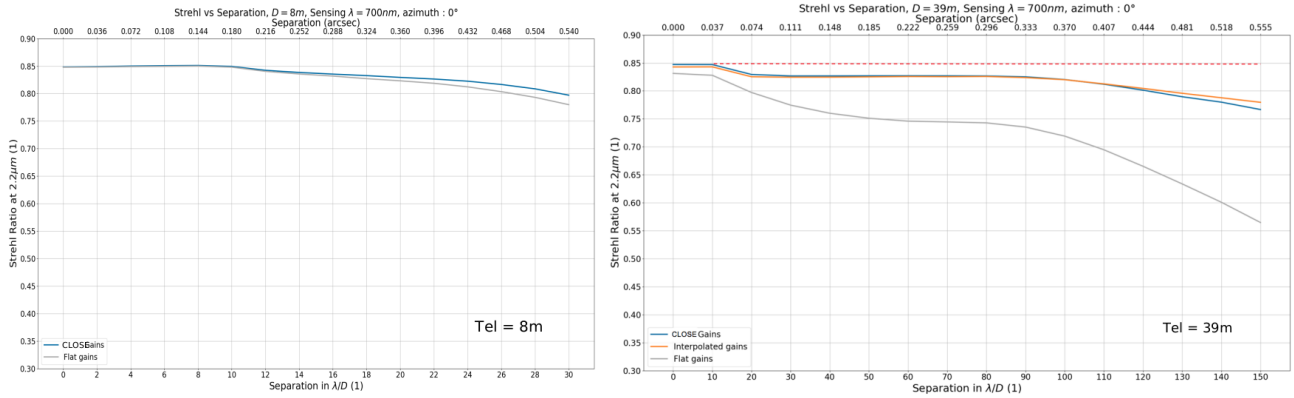
Figure 9. AO performance (SR in K Band) for PWFS system sensing on a double star Vs double star separation (in λ/D units or arcsecs). *Left*: 8m telescope case, *Right*: 39m telescope case (MICADO SCAO like). Each case is simulated *without* (grey = FLAT gains) and *with* optical gain compensation (CLOSE in blue and interpolated in orange))

and $100\lambda/D$ and is explained by the AO correction zone still crossing on 1 axis of the Pyramid edge. The final regime occurs when the AO correction zone does not even cross the pyramid edge and the wavefront sensing is completely decorrelated from the AO correction and the performance decreases quickly.
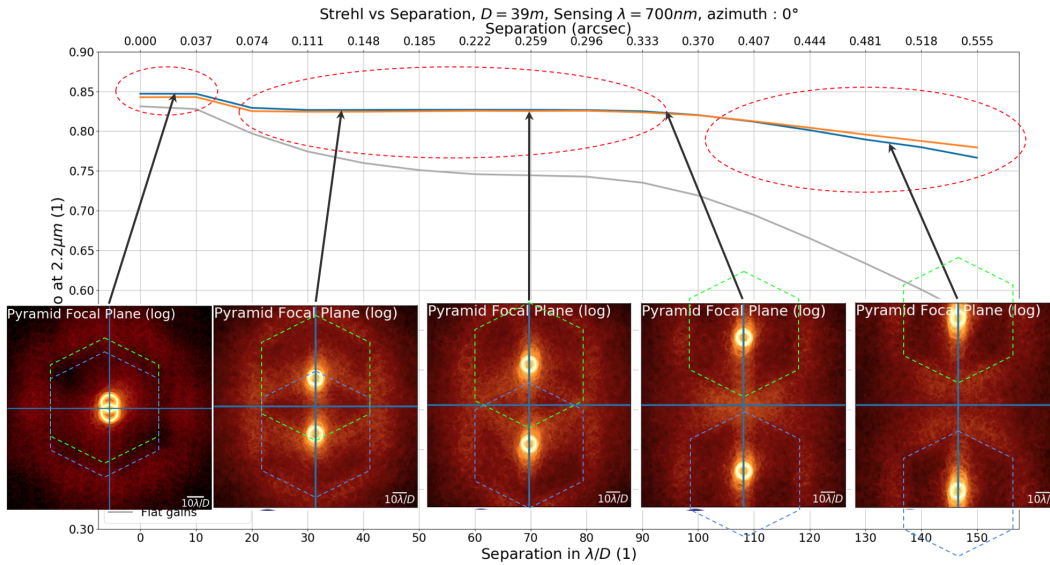

Figure 10. Illustration of the 3 regimes of performance depending on the double star position at the PWFS focal plane.

We now explore the case when the azimuth angle range from 0 to 45 degrees (rotation w.r.t pyramid edges). Figure 11 shows the AO performance on a 39m telescope for separations up to $150\lambda/D$ *without* optical gain compensation (FLAT modal gains). As soon as the azimuth angle is above 10 degrees the performance drops and degrades progressively as the azimuth angle increases. This is explained by the fact that the entire modulated PSF core always misses the edges of the Pyramid and the wavefront sensing is now affected on both x and y axes. At a separation of 0.54" the SR is now 34% ($\approx$ 50% SR loss).

The optical gain compensation dramatically helps to reduce the loss of performance. This is presented in Figure 11 where, by using CLOSE to measure the optical gain we improve the performance at SR=72% (+38
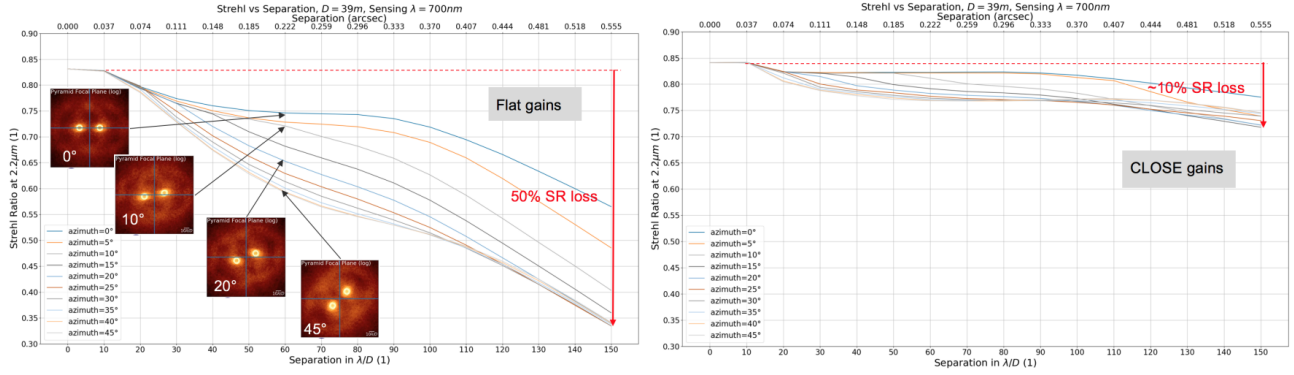
Figure 11. SCAO PWFS system sensing on a double star on a 39m telescope (MICADO SCAO case). AO performance (SR in K Band) Vs double star separation (in λ/D units or arcsecs) and azimuth angle without (FLAT) optical gain compensation.

SR points) at a maximum separation of 0.54". We also see that compensating the optical gain removes the azimuth angle dependency on the AO performance. A video illustrating the stabilization of the AO performance while the double star separation and azimuth angle changes is also available[17] . Finally, although the results presented in this section were performed with an equal illumination of both components, we also studied the impact of brightness difference. We found that when the faintest star has a difference of magnitude >1.75 the AO performance is no more affected by this component and the system behaves and delivers the same performance as a single star.

7.3 Sensing on Titan

We simulate in this section the case when Titan is used as the PWFS wavefront sensing source. Such a simulation is quite heavy computing (33317 modulation points) therefore we tested only 2 cases. First is *without* optical gain compensation (FLAT gains). The SCAO performance then gives 61.9% SR after 3000 iterations of the AO loop (5 seconds of real observation at 500Hz). The second case used CLOSE to measure and compensate for the optical gains and SCAO delivers now 82% SR. Such a simulation is illustrated in Figure 12. A video of this simulation is also available[18] .

8. CONCLUSION

We presented the optimizations performed to deal with PWFS specific calibrations expected at the telescope (optical gain , NCPA management, island effect). We also presented a detailed error budget for each of the 5 turbulence conditions (seeing from 0.47" to 1.13") and guide star magnitudes between 10 to 17 with an unresolved single star. The MICADO SCAO performance at magnitude 10 gives Strehl Ratio of 68.8% in K Band which is above the 60% specification. We also studied the impact of extended objects such as double stars on Pyramid wavefront sensing. We performed exploration of the parameter space in particular when the 2 components moves with respect to the pyramid edges (separation and rotation). We found that using optical gain compensation is mandatory for a SCAO system on a ELT sensing using an equal brightness double star. This calibration improves the AO performance by more than 40% SR points for the most extreme cases. We also studied the case of large resolved source disk such as Titan and found the optical gain compensation allows to reach the same level of performance than a single star.

REFERENCES

[1] Davies, R., Schubert, J., Hartl, M., Alves, J., Clénet, Y. et al., "MICADO: first light imager for the E-ELT", Proceedings of the SPIE, Volume 9908, id. 99081Z 12 pp. (2016)

[2] Diolaiti E., Ciliegi, P., Abicca, R., Agapito, G., Arcidiacono, C et al., "MAORY: adaptive optics module for the E-ELT" Proceedings of the SPIE, Volume 9909, id. 99092D 7 pp. (2016)
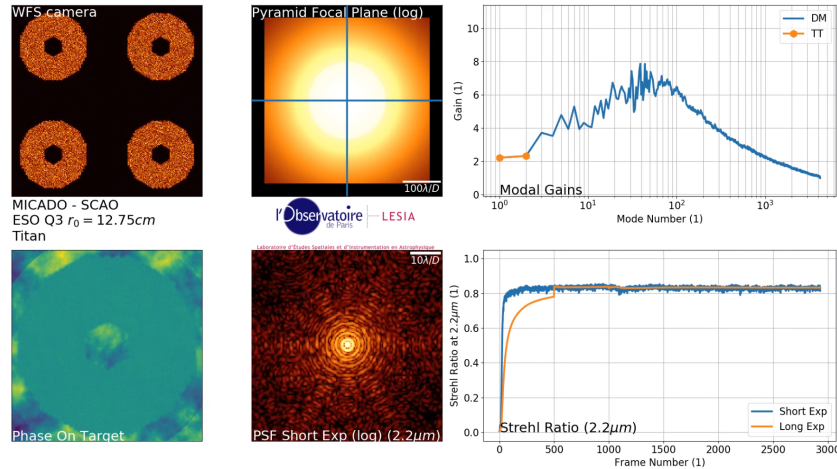
Figure 12. SCAO PWFS system sensing on a Titan after 3000 iterations (6 seconds of SCAO loop) with optical gain compensation using CLOSE. Top left: PWFS raw image. Top center: PWFS focal plane image in the visible. Top right: modal gain as measured and applied by CLOSE. Bottom left: wavefront residuals. Top center: Corrected PSF (K Band). Bottom right: short and long exposure SR in K Band as function of time (final long exposure SR= 82%).

[3] https://anr-compass.github.io/compass/

[4] Vernet, E., Cayrel, M., Hubin, N. Mueller, M. Biasi, R., "Specifications and design of the E-ELT M4 adaptive unit", Proceedings of the SPIE, Volume 8447, article id. 844761, 8 pp. (2012)

[5] Schwartz N., "Sensing and control of segmented mirrors with a Pyramid wavefront sensor", This conference.

[6] R. Ragazzoni and J. Farinato, "Sensitivity of a pyramidic Wave Front sensor in closed loop Adaptive Optics", Astron. & Astrophys. 350, L23-L26 (1999)

[7] V. Viotto, R. Ragazzoni, M. Bergomi, D. Magrin, and J. Farinato, "Expected gain in the pyramid wavefront sensor with limited Strehl ratio", A&A 593, A100 (2016)

[8] Korkiakoski, V. , Vérinaud, C and Le Louarn, M., "Improving the performance of a pyramid wavefront sensor with modal sensitivity compensation", Applied Optics, Vol. 41, 1, pp 79-87 (2008)

[9] N. Jovanovic, F. Martinache, O. Guyon et al., "The subaru coronographic extreme adaptive optics system: enabling high-contrast imaging on solar-system scales.", PASP, (2015), 127, 890

[10] S. Esposito, A. Riccardi, E. Pinna et al., "Large binocular telescope adaptive optics system: new achievements and perspectives in adaptive optics", Proc of SPIE, Volume 8149, pp. 814902-814902-10 (2011)

[11] Deo, V., Gendron, É., Rousset, G. et al. "Assessing and mitigating alignment defects of the pyramid wavefront sensor: a translation insensitive control method", A& A, Volume 619, id.A56, 13 pp. (2018)

[12] Esposito S, Pinna E, Puglisi A, et al. 2015, "Non common path aberration correction with non linear WFSs", in 4th AO4ELT conference proceedings.

[13] Deo V., Gendron É., Rousset G. et al. "A telescope-ready approach for modal compensation of pyramid wavefront sensor optical gain", A&A, Volume 629, id.A107, 18 pp. (2019)

[14] Chambouleyron V ,Fauvarque O,Janin-Potiron P., Schatz L. Brûlé Y., Neichel, B., Correia C., Sauvage J.F. and Fusco, T., "Modal gain optimization of the Pyramid Wave-Front Sensor using a convolutive model: from theory to experimental validation" AO4ELT6 conference proceedings held in Quebec (2019)

[15] V. Deo, M. Rozel, A. Bertrou-Cantou, F. Ferreira, F. Vidal, D. Gratadour, A. Sevin, Y. Clénet, G. Rousset, and É. Gendron, "CLOSE: a self-regulating, best-performance tracker for modal integrator based AO loops", AO4ELT6 conference proceedings held in Quebec (2019)

[16] A.Bertrou-Cantou, E.Gendron, G.Rousset, F.Vidal, V.Deo, and F.Ferreira, "Analysis of the island effect for ELT MICADO MAORY SCAO mode", AO4ELT6 conference proceedings held in Quebec (2019)

[17] https://tinyurl.com/doubleStarCLOSE

[18] https://tinyurl.com/TitanCLOSE